Electronic structure and magnetic properties of cubic and hexagonal $SrMnO_3$

Rune Søndenå, P. Ravindran, and Svein Stølen*
Department of Chemistry and Centre for Materials Science and Nanotechnology, University of Oslo, Postbox 1033 Blindern, N-0315 Oslo, Norway

Tor Grande
Department of Materials Science and Engineering, Norwegian University of Science and Technology, N-7491 Trondheim, Norway

Michael Hanfland
European Synchrotron Radiation Facility, Boîte Postale 220, F-38043 Grenoble, France
(Received 20 June 2006; revised manuscript received 17 August 2006; published 4 October 2006)

$SrMnO_3$ is a rare example of a compound having both a cubic (high-temperature) and a hexagonal (low-temperature) perovskite polymorph. While the former is built from corner-sharing MnO_6 octahedra only, the latter contains corner-sharing confacial bioctahedral Mn_2O_9 entities along the *c* axis. The electronic and magnetic structures of both polymorphs are investigated by density functional theory. Both the cubic and the hexagonal polymorphs are insulators at 0 K but with quite different band gaps (0.3 vs 1.6 eV). The hexagonal ground state shows antiferromagnetic coupling both within the Mn_2O_9 entities and between the Mn ions in the corner-sharing octahedra. The lowest energy cubic configuration is found to be *G*-type antiferromagnetic and is 260 meV per formula unit higher in energy than the hexagonal ground-state structure. While the bonding interactions involving Sr are found to be mainly ionic, there is a significant covalent contribution to the Mn-O bond. This covalency is very important for the stabilization of the hexagonal structure compared to the cubic polymorph. Two additional factors that stabilize hexagonal $SrMnO_3$ relative to the cubic polymorph are identified. (i) the Mn atoms in the face-sharing octahedra are displaced along the *c* axis by about 0.012 Å from the center of the octahedra. (ii) The charge transfer giving lower charges for the oxygen in the face-sharing triangle compared to the corner-sharing oxygen. The latter effect results in a contraction of the oxygen triangle in the shared face. This negatively charged oxygen triangle effectively shields the repulsive interaction between the manganese atoms in the Mn_2O_9 dimer and facilitates the short Mn-Mn distance present in hexagonal $SrMnO_3$. Hexagonal $SrMnO_3$ is more compressible than cubic $SrMnO_3$, owing to the more open structure. The calculated bulk modulus for hexagonal $SrMnO_3$ is in good agreement with the high-pressure powder x-ray diffraction measurements also reported in the present paper.

DOI: 10.1103/PhysRevB.74.144102 PACS number(s): 71.15.Nc, 75.25.+z, 71.20.Ps, 61.50.Ah

I. INTRODUCTION

The perovskite structure, ABX_3, has been termed an *inorganic chameleon* due to the large flexibility of the structure. Many different compounds take this or a related structure since the mother structure easily distorts or adapts to the relative sizes of the ions forming the compound.[1] Hexagonal perovskites in which octahedra share faces and form chains along the hexagonal *c* axis are less common than cubic perovskites, where all octahedra share corners, and typically form when the *A* cations are too large to be accommodated in the *A* site of the BX_3 framework. In such cases the cations at the *A* site alternatively can be placed between columns of face-shared octahedra. However, the face-sharing octahedra increase the electrostatic repulsion between the two *B*-site cations involved, and therefore increase the Madelung energy of the compound. Thus hexagonal stacking is introduced in stages with the increasing size of the *A* cation. Alkali-earth manganese oxides, $AeMnO_3$, reflect this importance of size well. The ionic radius of the alkali earth ion increases from Ca^{2+} ($r_{Ca^{2+}}=1.98$ Å), to Sr^{2+} ($r_{Sr^{2+}}=2.15$ Å), and Ba^{2+} ($r_{Ba^{2+}}=2.24$ Å) and while $CaMnO_3$ forms an orthorhombic derivative of the ideal cubic structure,[2] $BaMnO_3$ crystallizes in a hexagonal structure in which all octahedra share faces along the *c* axis (2*H*-type).[3] $SrMnO_3$, containing intermediately sized Sr^{2+} ions, is a rare example of a compound having both cubic and hexagonal polymorphs.[4] The latter is a 4*H* type with alternating face-sharing and corner-sharing MnO_6 octahedra along the *c* axis. The hexagonal modification is stable up to about 1035 °C where it transforms into a cubic high-temperature modification.[5] The enthalpy of transition is about 6 ± 2 kJ mol^{-1}.[6]

Hexagonal $SrMnO_3$ is antiferromagnetic below the Néel temperature (T_N).[7] A detailed magnetic structure has not yet been determined and this motivated us to undertake a detailed analysis of the magnetic properties. The discrepancy between the early reported ($T_N=350$ K)[3] and more recently reported ($T_N=278\pm5$ K) has been interpreted as a result of short-range antiferromagnetic (AF) coupling between Mn ions in face-sharing MnO_6 octahedra above T_N. No long-range magnetic ordering is observed at 290 K.[7] However, the difference in T_N may alternatively be associated with differences in oxygen stoichiometry between the samples used (see below). High-temperature cubic $SrMnO_3$ can be quenched and maintained as a metastable compound at low temperatures. Cubic $SrMnO_3$ adopts a *G*-type[8] AF structure at low temperatures and the magnetic moment at the Mn site is found to be $2.6\pm0.2\mu_B$ at liquid nitrogen temperature.[9] The Néel temperature is reported to be 260 K by Takeda and

Ohara[9] while more recent results by Kikuchi *et al.*[10] and Chmaissem *et al.*[11] give 250 and 233 K, respectively. The difference in T_N is probably caused by differences in the oxygen stoichiometry of the samples also here.

Both the hexagonal and the cubic polymorphs are semiconductors. The electronic properties are, however, largely affected by stoichiometry. Hexagonal $SrMnO_3$ when heated in air is stoichiometric at room temperature but loses oxygen at high temperatures and has composition $SrMnO_{2.89}$ at the transition to the cubic polymorph at around 1400 °C.[12] Similarly, the cubic modification is largely nonstoichiometric and cubic $SrMnO_{2.62}$ obtained on quenching from 1740 °C is reoxidized at around 300 °C to produce stoichiometric cubic $SrMnO_3$. Hence, experimental data must be treated with care, and the characterization of the oxygen deficiency of the sample is important. Hexagonal $SrMnO_3$ produced by annealing in air at 900 °C show semiconducting behavior and the conductivity varies from $6.0-10^{-6}$ S cm^{-1} at room temperature to 0.5 S cm^{-1} at 1000 °C.[13] The electric conductivity of cubic $SrMnO_3$ varies very little in the temperature range from 100 to 300 K, approximately from 10^{-2} S cm^{-1} to 0.5 S cm^{-1}.[14] A larger band gap for the hexagonal modification is inferred.

The nature of the band gap has been investigated both experimentally and theoretically and there is some discussion on whether $SrMnO_3$ and its close relative $CaMnO_3$ are in the Mott-Hubbard or charge-transfer regime. In oxides of the early first series transition metals (Ti and V) the band gap is a *d-d* gap where the direct Coulomb repulsion between electrons in the same orbitals U is clearly smaller than the *p-d* charge transfer energy Δ. Oxides of the late first series transition metals (Cu and Ni) on the other hand, have charge-transfer type band gaps since the order of energy is reversed; $\Delta < U$.[15] This has been shown by a range of studies using different spectroscopic techniques that have focused largely on the effect of hole doping of early and late transition metal oxides. The $3d^n$ ground state of the undoped compound becomes d^n and $3d^{n-1}$ for early transition metals ($U<\Delta$) and $3d^n\underline{L}$ for late transition metals ($U>\Delta$), where $\underline{L}$ denotes a ligand hole. For $U=\Delta$ the states will be of heavily mixed character. Manganese oxides being in the intermediate region of the Zaanen, Sawatzky, Allen phase diagram[15] represent less clear-cut cases.[16] From spectroscopic measurements Abbate *et al.*[17] and Chainani *et al.*[18] suggested heavily mixed ground states for $La_{1-x}Sr_xMnO_3$. On the other hand, Saitoh *et al.*[19] and Zampieri *et al.*[20] proposed a band gap that to a large extent is of the charge-transfer type for $SrMnO_3$ and $CaMnO_3$.

First-principles band-structure calculations suggest that cubic *G*-type antiferromagnetically ordered $SrMnO_3$ is an insulator (at 0 K) with a small band gap.[21] The nature of the band gap was not discussed, but the results agree with the electronic structure of the cubic and orthorhombic modifications of the related compound $CaMnO_3$. The ideal cubic $CaMnO_3$ is also found to be a *G*-type antiferromagnetically ordered insulator.[2,22] In a more recent study of $SrMnO_3$ a finite contribution to the electronic density of state in a one-spin direction at the Fermi energy was obtained, hence suggesting half-metallic behavior.[23] The magnetic ordering considered in this study was, however, not clearly stated. The features of the band structure appear to be those of a ferromagnetic state.

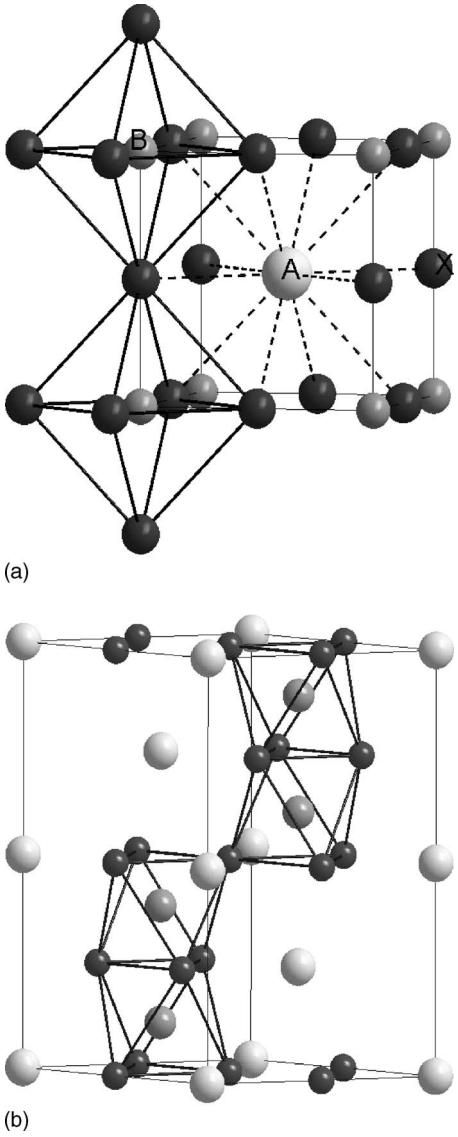

FIG. 1. The polyhedron representations of (a) the ideal cubic perovskite and (b) the four-layer hexagonal perovskite structures.

The present paper focuses on the electronic contributions to the phase stability of the two $SrMnO_3$ polymorphs through first-principles density functional theory (DFT). Complementary high-pressure powder x-ray diffraction data for hexagonal $SrMnO_3$ are also reported. These data are used to derive an experimental value for the bulk modulus which again is used to test the quality of the band-structure calculations. A subsequent paper will report on the lattice dynamics (experiments and calculations) and hence the vibrational entropy contribution to the phase stability.

II. CRYSTAL AND MAGNETIC STRUCTURES

The crystallographic structures of the two $SrMnO_3$ polymorphs considered are given in Fig. 1. The representation of the ideal cubic perovskite structure of $SrMnO_3$ (space group

$Pm\bar{3}m$)[9] in Fig. 1(a) shows the coordination polyhedra of the Sr- and Mn-site cations. The lattice sites remain in the ideal cubic perovskite positions with Sr in (0,0,0), Mn in $(\frac{1}{2},\frac{1}{2},\frac{1}{2})$ and O in $(\frac{1}{2},\frac{1}{2},0)$. While the *A* cations are surrounded by twelve anions in a cubo-octahedral coordination, the *B* cations are surrounded by six anions in octahedral coordination. The O anions are coordinated by two *B*-site cations and four *A*-site cations. $SrMnO_3$ alternatively takes a hexagonal perovskite-type structure at low temperatures; a 4*H* polytype in which four layers of manganese are stacked along the *c* direction of the cell, where *H* indicates hexagonal symmetry.[7,24] A polyhedron representation of the 4*H* polytype is given in Fig. 1(b). The face-sharing octahedra give rise to Mn_2O_9 dimers, with a Mn-Mn distance close to that in metallic manganese.

Turning to the magnetic structures, the situation becomes more complicated. Several magnetically ordered structures are in general possible for cubic perovskites depending on the exchange interactions between neighboring *B*-site cations (*B*-O-*B* interactions) within a defined plane (intraplane) and between planes (interplane).[8] The ferromagnetic (F) structure results when both interplane and intraplane interactions are ferromagnetic. While antiferromagnetic interplanar and ferromagnetic intraplanar coupling lead to *A*-type AF order, the opposite situation (AF intraplanar and F interplanar coupling) gives *C*-type AF. In cases where both interactions are antiferromagnetic, *G*-type AF order result. These four types of magnetic order considered computationally here are given in Fig. 2(a). Experiments suggest that cubic $SrMnO_3$ takes the *G*-type AF state.[9]

While the crystallographic structure of the hexagonal polymorph is well characterized, this is not so for the magnetic structure. 4*H* $SrMnO_3$ is AF magnetically ordered but the detailed structure is unknown.[7] Here we confine our discussions to the nonspin polarized (NSP) state, the ferromagnetically ordered state, as well as the two AF magnetically ordered states shown in Fig. 2(b). The magnetic ordering of the 4*H* modification of $BaMnO_3$ has by neutron diffraction been found to be antiferromagnetic with alternating spins along the *c* axis (both within the Mn_2O_9 dimers and between the corner-sharing MnO_6 octahedra) and with spins parallel to the *a* axis (termed AF1 in the present paper).[25] The same magnetic structure has been found for 4*H* $Ba_{0.1}Sr_{0.9}MnO_{2.96}$.[26] Other Mn-containing hexagonal perovskite oxides, like $SrMn_{1-x}Fe_xO_{3-\delta}$[27] and $BaIr_xMn_{1-x}O_3$,[28] also show the same feature with antiferromagnetic coupling along the *c* axis. In addition to this AF1 ordering that we consider the most probable, an antiferromagnetic structure with ferromagnetic coupling within each Mn_2O_9 dimer (AF2) is investigated here. Such a magnetic structure has recently been observed in 6*H* perovskitelike $Ca_3Co_2O_6$ by low-temperature neutron diffraction.[29]

III. COMPUTATIONAL DETAILS

In most of our calculations we have used the projector augmented wave (PAW)[30] implementation of the Vienna *ab initio* simulation package (VASP).[31–33] The self-consistent calculations are performed using the generalized gradient approximation (GGA).[34] The cutoff energy for the plane-wave basis is 500 eV. Periodic unit cells of 10 (5 for NSP) lattice sites for the various cubic structures, and 20 lattice sites for the hexagonal cell are used. To ensure high accuracy, the *k*-point density and the plane-wave cutoff energy are increased until convergence. The *k*-point densities used in the final optimizations were $19\times19\times19$ for cubic and $13\times13\times8$ for hexagonal $SrMnO_3$. While the Monkhorst-Pack mesh is used for the cubic unit cell, a Γ-centered *k*-point mesh is used for the hexagonal cell. For NSP calculations the total electron population is accounted for in the potential, while in spin-polarized calculations, a magnetic moment is allowed to appear on an atomic species when majority and minority spin electrons are treated separately.

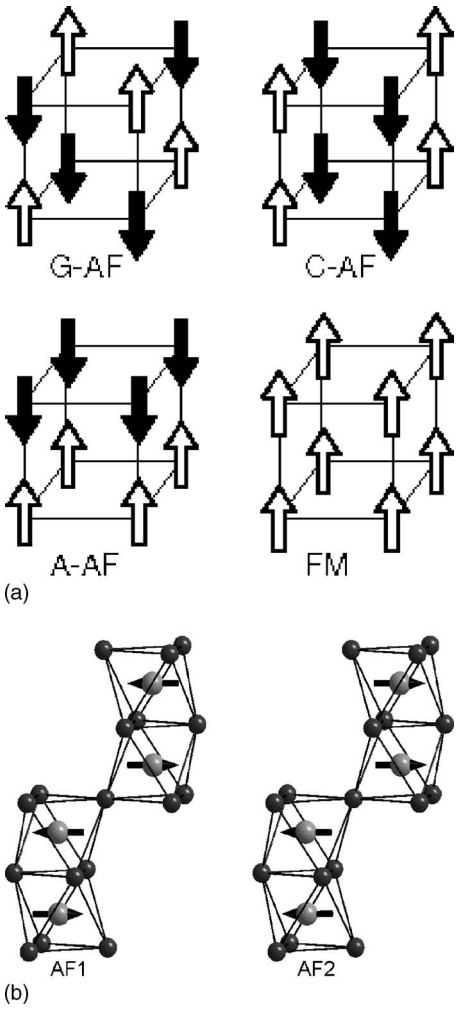

FIG. 2. The four magnetic configurations considered for (a) cubic $SrMnO_3$ and the two AF configurations considered for (b) hexagonal $SrMnO_3$.

The Birch-Murnaghan equation of state

$$V(P) = V_0\left(1+\frac{B_0'}{B_0}P\right)^{-1/B_0'} \quad (1)$$

is used to calculate the bulk modulus B_0 and its derivative B_0' from experimental high-pressure powder x-ray diffraction data. This equation can be rewritten in the form

TABLE I. The total energy, unit-cell dimensions, and magnetic moment of hexagonal $SrMnO_3$.

Configuration	E (meV)	a (Å)	c (Å)	M_{Mn} (μ_B)	M_{cell} (μ_B)
Present calculations					
NSP	809	5.469	8.914		
F	224	5.514	9.175	2.67	2.89
AF2	23	5.489	9.132	2.51	0
AF1	0	5.489	9.114	2.47	0
Experimental values					
Chamberland *et al.* (Ref. 3)		5.449	9.080		
Negas & Roth (Ref. 12)		5.449	9.078		
Battle *et al.* (Ref. 7)		5.4434	9.0704		
Kuroda *et al.* (Ref. 24)		5.454	9.092		
Syono *et al.* (Ref. 4)		5.449	9.085		

$$P(V) = \frac{B_0}{B_0'}\left[\left(\frac{V_0}{V}\right)^{B_0'} - 1\right] \tag{2}$$

which by integration, $E=E_0-\int PdV$, gives the Birch-Murnaghan equation of state for $E(V)$,[35,36]

$$E(V) = E_0 + \frac{B_0 V}{B_0'}\left(\frac{(V_0/V)^{B_0'}}{B_0'-1} + 1\right) - \frac{B_0 V_0}{B_0'-1}. \tag{3}$$

The bulk modulus is derived by calculating the total energy at different volumes allowing all atomic positions to vary. In the hexagonal case also the a and c values are varied while keeping the volume fixed.

In order to illustrate the character of the bonding in more detail we have calculated the crystal orbital Hamiltonian population (COHP)[37] for cubic $SrMnO_3$ (G-type AF-state). The COHP is a density of states weighted by the corresponding Hamiltonian matrix elements where negative values indicate bonding, and positive values indicate antibonding states. The COHP's are calculated using the tight-binding (TB) linear muffin-tin orbital (LMTO) method[38,39] which gives a band structure in good accord with that obtained by VASP.

IV. EXPERIMENTAL DETAILS

A. Synthesis and characterization

$SrMnO_3$ was synthesized by the EDTA precursor method. $Sr(NO_3)_2$ (>99%, Merck), and $Mn(NO_3)_2 \cdot 4H_2O$ (>98.5%, Merck) were heat-treated at temperatures between 700 and 1100 °C to determine the exact amount of crystal water in the nitrates. Stoichiometric amounts of nitrates were dissolved in ion-exchanged water, then an EDTA (ethylendiamine-tetraacetic acid, 99.7%, Sigma) solution (0.8 M and pH 8–9) was added, and the final solution was heated on a hot plate to 80±3 °C. The solution was continuously stirred at 80 °C until a gel was formed. The pH was controlled during heating, and NH_3 (concentrated) was added to keep the pH at 7–11, depending on the type of ions in the solution. The gel was dried overnight at 150–200 °C and fired at approximately 500 °C to remove all the organic matter. $SrMnO_3$ was calcined at 1100 °C for 72 h. Single phase hexagonal $SrMnO_3$ was identified by x-ray diffraction (SIEMENS D5000 or D5005, Siemens Germany) using Cu $K\alpha$ radiation. Silicon was used as an internal standard to determine the unit cell dimensions.

B. High-pressure x-ray diffraction

X-ray diffraction measurements under pressure were performed at room temperature in a membrane-type diamond anvil cell with the sample loaded in a hole in a stainless steel gasket with a diameter of 125 μm and an initial thickness of 40 μm. Nitrogen was used as a pressure-transmitting medium. It solidifies at 2.3 GPa at ambient temperature[40] and three crystalline modifications of nitrogen are reported at high pressure. The disordered hexagonal low-pressure structure[41] transforms into a disordered cubic structure between 4 and 5 GPa,[42] which again transforms to an ordered rhombohedral modification near 16 GPa.[40] The rhombohedral modification is stable at least to 44 GPa.[43] Pressure was measured by the ruby fluorescence technique using the nonlinear hydrostatic pressure scale.[44]

Powder x-ray diffraction data were collected on beamline ID9 at the European Synchrotron Radiation Facility (ESRF). The diffractograms were collected on an image plate, scanned, and thereafter integrated with the computer program FIT2D[45] and thereby transformed to a one-dimensional data set. The monochromator was a single reflection Si(111) monochromator with a wavelength of $\lambda = 47.68 \pm 0.04$ pm. The 2D image plate distance and the wavelength were calibrated using Si in a separate experiment. The conical opening of the pressure cell allowed the observation of the full diffraction rings for $d > 95$ pm.

V. RESULTS AND DISCUSSION

A. Crystal structures

The results of the total energy calculations for different magnetic configurations of hexagonal $SrMnO_3$ are presented in Table I. For each configuration, the shape and volume of the unit cell as well as the atomic coordinates are optimized.

TABLE II. Atomic coordinates of hexagonal AF1-type $SrMnO_3$.

$P6_3/mmc$	Wyck.	Expt. (Ref. 7) a=5.4434, c=9.0704 Å			Present calc. a=5.489, c=9.114 Å		
		x	y	z	x	y	z
Sr1	2a	0	0	0	0	0	0
Sr2	2c	1/3	2/3	1/4	1/3	2/3	1/4
Mn	4f	1/3	2/3	0.6122	1/3	2/3	0.6129
O1	6g	1/2	0	0	1/2	0	0
O2	6h	−0.1807	−0.3614	1/4	−0.1805	−0.3611	1/4

The magnetic configuration with antiferromagnetic coupling both within the Mn_2O_9 entities and between the Mn ions in the corner-sharing octahedra (AF1) has the lowest energy, and is assumed to be the ground state. AF2 with ferromagnetic coupling within the dimers lies 23 meV per formula unit higher in energy than the ground state. The hypothetical ferromagnetic and the NSP states are 224 and 809 meV per formula unit higher in energy than the ground state. For the spin-polarized cases, Table I also presents calculated values for the magnetic moment per manganese atom. The calculated magnetic moment, $2.47\mu_B$ per Mn, for hexagonal $SrMnO_3$ in the antiferromagnetic ground state agree reasonably well with the magnetic moment for Mn in the closely related 4*H* $Ba_{0.1}Sr_{0.9}MnO_{2.96}$, $2.41\mu_B$.[26]

The optimized unit-cell dimensions for hexagonal $SrMnO_3$ are compared with available experimental values in Table I. The calculated unit-cell dimensions for the ground state are in good agreement with the experimental values. In general, the equilibrium volumes calculated using GGA are overestimated, and agreement with experiments within 2% is considered good. Calculated and experimental atomic coordinates are given in Table II. The excellent agreement for the magnetic ground state of hexagonal $SrMnO_3$ indicates that the state-of-the-art density functional calculations can reliably be used to predict structural parameters even for compounds with relatively complex structures.

Calculated total energies and unit-cell dimensions for different magnetic configurations of cubic $SrMnO_3$ are presented in Table III. The nonspin polarized state lies highest in energy also for cubic $SrMnO_3$. All the different antiferromagnetic states are more energetically favorable than the ferromagnetic ordering due to super exchange via oxygen *p* orbitals (see below). In the calculations there were no restrictions on atomic coordinates nor on the shape and volume of the unit cells used in the optimizations, and the *A*- and *C*-type AF ordered unit cells relax into tetragonal symmetry (although only slightly elongated along the *c* axes). The ground state of cubic $SrMnO_3$ is found to be the *G*-type AF ordered state. It lies 260 meV per formula unit higher in energy than the hexagonal ground state, in agreement with the fact that hexagonal $SrMnO_3$ is stable at low temperatures. This calculated enthalpy of transition is about 19 kJ mol^{-1} higher than the experimental value. The calculated magnetic moment for the Mn ions in the magnetic ground state of cubic $SrMnO_3$ is as for the hexagonal ground state found to be $2.47\mu_B$. This lies well within the uncertainty of the experimental value.[9] In general, the total energies are higher for the NSP configurations than for the spin-polarized ones for both cubic and hexagonal $SrMnO_3$. For both polymorphs the ferromagnetic state lies higher in energy than all antiferromagnetic states.

First-principles calculations have previously been performed for the closely related compound $CaMnO_3$,[46–48] both for the cubic perovskite structure, and for the ground-state orthorhombic modification. The calculated energy differences are shown in Table IV. Also for cubic $CaMnO_3$ the

TABLE III. The total energy, unit-cell dimensions, and magnetic moment of cubic $SrMnO_3$.

Configuration	Space group	E (meV)	a (Å)	c (Å)	M_{Mn} (μ_B)
Present calculations:					
NSP	$Pm\bar{3}m$	850	3.801		
Ferromagnetic	$Pm\bar{3}m$	128	3.839		2.616
A-type AF	$P4/mmm$	78	3.85	3.79	2.52
C-type AF	$Cmmm$	25	3.81	3.87	2.48
G-type AF	$Pm\bar{3}m$	0	3.824		2.47
Earlier reported calculations:					
Fuks *et al.* (Ref. 23)			3.845		
Expt.:					
Negas & Roth (Ref. 12)			3.806		
Takeda & Ōhara (Ref. 9)			3.80		2.6±0.2
Chmaissem *et al.* (Ref. 11)			3.805		

TABLE IV. The total energy of different magnetic configurations of cubic and orthorhombic $CaMnO_3$ as reported in the literature.

	Cubic $CaMnO_3$			Orthorhombic $CaMnO_3$	
	Pickett and Singh (Ref. 46)	Nicastro and Patterson (Ref. 47)	Matar (Ref. 48)		Matar (Ref. 48)
NSP	860 meV		955 meV	NSP	816 meV
F	116 meV	64 meV	217 meV	F	56 meV
A	60 meV	41 meV	139 meV	AF	0 meV
C		19 meV			
G	0 meV	0 meV	0 meV		

G-type AF state is found to be lowest in energy among the different magnetic configurations.[49] The energy differences are of a similar order of magnitude as we observe here for $SrMnO_3$, although they vary somewhat since the cation radii of calcium and strontium are different. This will influence the exchange interactions. The overall agreement between the present and the earlier studies must be considered good.

The origin of the magnetic ground states deserves additional discussion. The calculated magnetic moment is for both modifications smaller than the spin-only moment expected for a purely ionic compound with d^3 configuration. This indicates some degree of covalent bonding. In cubic $SrMnO_3$ the spins of the Mn atoms align antiferromagnetically due to linear Mn-O-Mn superexchange interactions. Two Mn atoms interact through the same oxygen *p* orbital causing antiparallel spins on neighboring Mn atoms. It is more difficult to rationalize the magnetic order obtained for hexagonal $SrMnO_3$. In the hexagonal structure we find the linear Mn-O-Mn superexchange interaction between Mn ions in the corner-sharing MnO_6 octahedra, and antiparallel spins result. When considering the face-sharing octahedra (the Mn_2O_9 dimer) we can initially focus on the O atoms surrounding the two Mn atoms. Two orthogonal oxygen *p* orbitals bonding to two Mn atoms will, according to Goodenough-Kanamori-Anderson (GKA) rules,[50–52] result in a weak ferromagnetic cation-anion-cation interaction. However, exceptions to this rule are seen, e.g., for some perovskites with face-sharing octahedra like $BaMnO_3$[25] and $Ba_{0.1}Sr_{0.9}MnO_{2.96}$,[26] and also for nonperovskites like $CuGeO_3$[53] and $LiNiO_2$.[54] There are several possible contributions to the stabilization of the antiferromagnetic coupling within the dimer. First of all, the GKA rules are based on 90° M-O-M interactions that imply that the antiferromagnetic coupling is zero since the electron transfer needed is forbidden by symmetry. In our case, the Mn-O-Mn angle significantly deviates from 90° (81.4°). In addition, the presence of Sr ions in the lattice cannot be neglected.[53] Thus it is not possible to point to one single factor giving this magnetic order.

B. Experimental and theoretical determination of the bulk modulus

The results of our high-pressure x-ray diffraction study of hexagonal $SrMnO_3$ are given in Fig. 3 which presents the experimentally determined reduced unit-cell dimensions as a function of pressure. The hexagonal structure is anisotropic and the unique axis is less compressible than the *a* axis due to the columns of face-sharing octahedra along the *c* axis. This is also observed in the DFT calculations and very good agreement with the experiments is obtained (see Fig. 3). Experimental values of the bulk modulus (136 GPa) and its pressure derivative (4.16) have been deduced from the variation of the resulting unit cell volume with pressure [using the Birch-Murnaghan equation of state, Eq. (1)]. The experimental (and calculated, see below) reduced volumes are given as a function of pressure in Fig. 4.

Values of the bulk modulus, B_0, and its pressure derivative, B_0', are calculated from the variation of the total energy with volume (see Fig. 5); both for cubic and hexagonal $SrMnO_3$. The Birch-Murnaghan equation of state [Eq. (3)] was used also here. Experimental and theoretical values of B_0 and B_0' for both modifications are given in Table V. The obtained values, $B_0=126$ GPa and $B_0'=4.4$, for hexagonal $SrMnO_3$ agree well with the experimental ones, while the bulk modulus of the cubic modification is larger ($B_0=166$ GPa) than that of hexagonal $SrMnO_3$. This can be understood by considering the crystal structures. The cubic

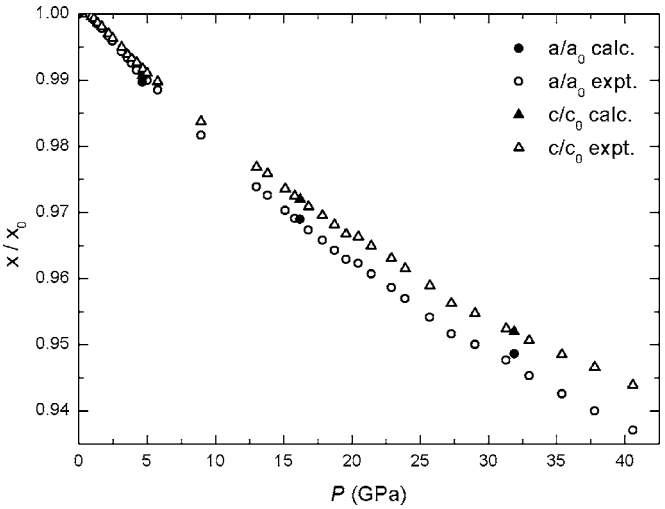

FIG. 3. The reduced unit-cell dimensions of hexagonal $SrMnO_3$ as a function of pressure. The open symbols represent experimental values determined by high-pressure x-ray diffraction; the filled symbols are calculated values.

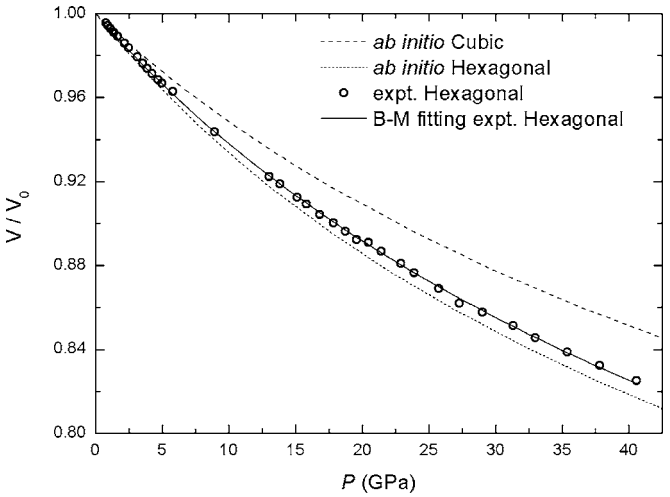

FIG. 4. The reduced volume of hexagonal and cubic $SrMnO_3$ as a function of pressure. The open circles represent experimental values for the hexagonal polymorph determined by high-pressure x-ray diffraction. The solid line represents a Birch-Murnaghan equation of state fit of the experimental data. The dashed and dotted lines represent the calculated values for cubic and hexagonal $SrMnO_3$, respectively.

structure consists of cubic close-packed layers normal to the [111] direction. The less dense hexagonal structure is not close packed, allowing an easier compression and a lower bulk modulus.

Since the density of cubic $SrMnO_3$ is higher than that of hexagonal $SrMnO_3$, a pressure-induced transition must be expected. It is calculated to take place at 12 GPa. Hence, the experimental determinations above 12 GPa represent measurements on metastable hexagonal $SrMnO_3$. Metastable $SrMnO_3$ is expected to transform to the stable modification on heating, giving the system sufficient kinetic energy for the transformation. Experiments confirming this were not made since the calculated transition pressure was not known when the experiments were made and since such experiments require special high-pressure cells or heating systems.

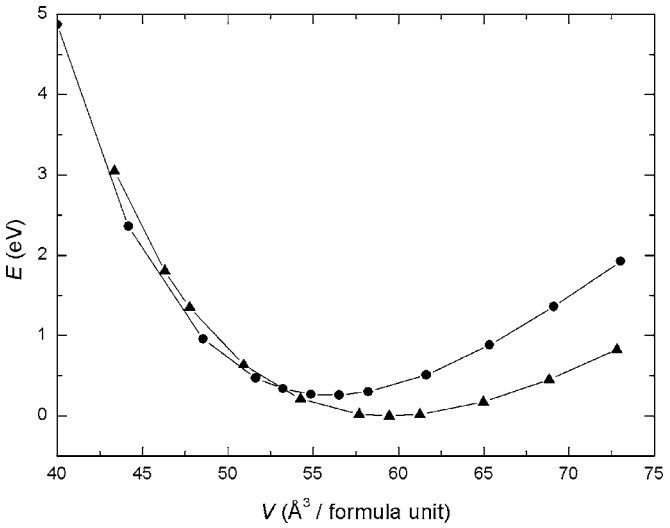

FIG. 5. The energy of cubic (solid circle) and hexagonal (solid triangle) ground-state structures as a function of the unit cell volume.

TABLE V. The experimental and calculated values of the bulk modulus and its pressure derivative.

	B_0 (GPa)	B_0'
Hexagonal AF1 $SrMnO_3$—calc.	126	4.40
Hexagonal $SrMnO_3$—expt.	136	4.16
Cubic *G*-type AF $SrMnO_3$—calc.	166	4.70
Cubic $SrMnO_3$—calc. (Ref. 23)	118.7	

C. Electronic structures

The total density of states (DoS) calculated for the different magnetic configurations considered for hexagonal $SrMnO_3$ are presented in Fig. 6. The nonspin-polarized configuration shows a substantial contribution $n(E)$ to the DoS at the Fermi energy (E_F). According to Stoner's criterion this indicates that spin-polarized calculations will yield an extra contribution to the stability.[49] Both antiferromagnetic (AF1 and AF2) states, as well as the ferromagnetic (F) state, have band gaps at the Fermi energy predicting insulating behavior at 0 K. The AF1 ground state has a band gap of approximately 1.60 eV. The following discussions for hexagonal $SrMnO_3$ will focus on this ground state. The fact that the ferromagnetic configuration is insulating is interesting also, since there are few solid ferromagnetic insulators. However, ferromagnetic insulating behavior has recently been reported for the electron doped (yttrium substituted) hexagonal perovskitelike compound $Ca_3Co_2O_6$.[55]

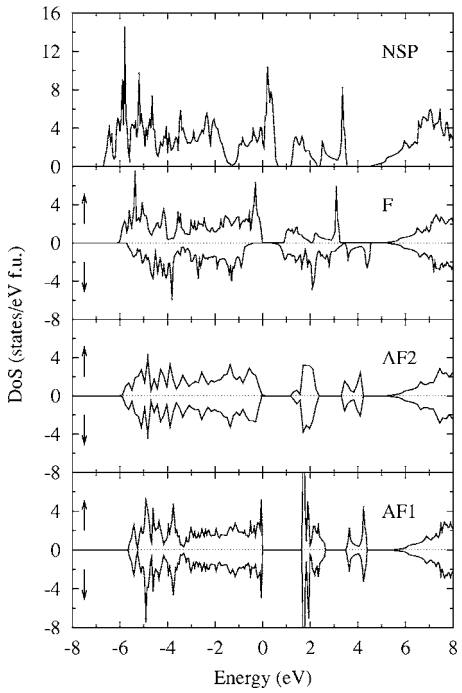

FIG. 6. The total electronic density of states for different configurations of hexagonal $SrMnO_3$.

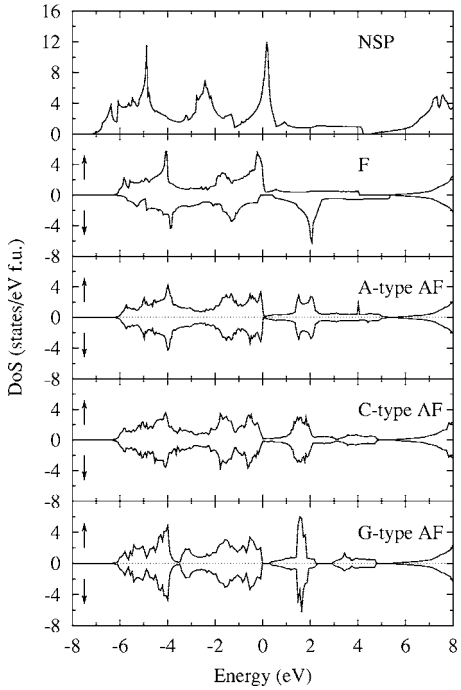

FIG. 7. The total electronic density of states for different configurations of cubic $SrMnO_3$.

Figure 7 shows the spin-projected total density of states for the different magnetic configurations considered for cubic $SrMnO_3$. The NSP calculation for cubic $SrMnO_3$ also shows a substantial contribution to the DoS at E_F. Half-metallic behavior is obtained for the ferromagnetic configuration; i.e., a finite contribution to the DoS at E_F for majority spin electrons, while the minority spin band shows an insulating gap of 0.6 eV over the Fermi energy. The resulting half-metallic properties may be of interest in connection with spintronics devices if the hypothetical ferromagnetic configuration can be stabilized. Both *A*- and *C*-type AF states have a small electron population at the E_F, and conducting properties are expected for both majority and minority spin electrons. The ground state *G*-type AF state is found to be an insulator with a band gap of approximately 0.30 eV. The following discussions for cubic $SrMnO_3$ will focus on this ground state.

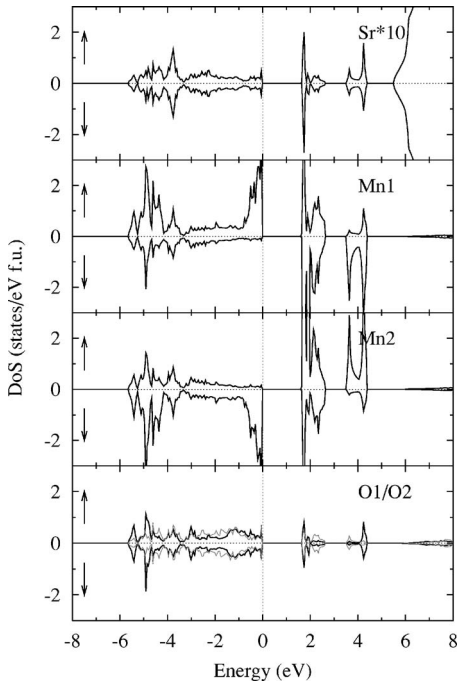

FIG. 8. The site-decomposed electronic density of states for AF1-type hexagonal $SrMnO_3$. Mn1 and Mn2 represent two different Mn atoms in the magnetic unit cell. O1 (dark line) represents oxygen atoms in the corner-sharing layer while O2 (gray line) represents oxygen atoms in the face-sharing layer.

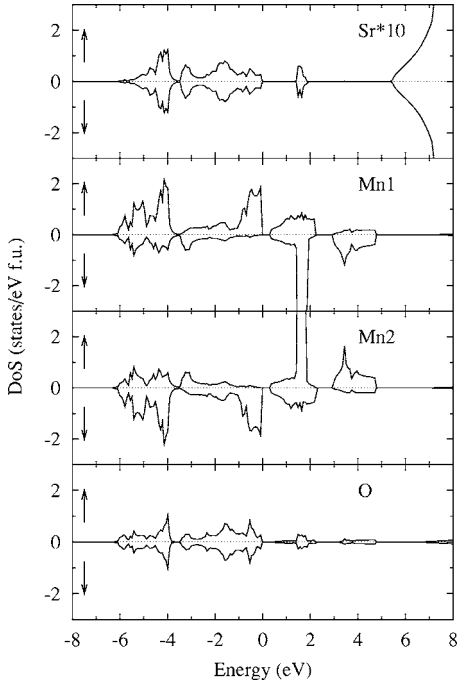

FIG. 9. The site-decomposed electronic density of states for *G*-type AF cubic $SrMnO_3$. Mn1 and Mn2 represent two different Mn atoms in the magnetic unit cell.

The electronic properties of all the magnetic configurations compare well with previous first-principles calculations for the corresponding magnetic structure for cubic $CaMnO_3$. Also here ferromagnetic $CaMnO_3$ was found to be half metallic, the *A*-type AF metallic and the *G*-type AF ground state insulating.[49]

The electronic band structures for both hexagonal and cubic $SrMnO_3$ in their magnetic ground states show band gaps over the Fermi energy, making both insulating at 0 K. Broader band gaps and higher more narrow peaks of electron states are seen for hexagonal $SrMnO_3$. Figures 8 and 9 show the spin and site decomposed DoS for the hexagonal and the cubic modifications in their magnetic ground states, respectively. The DoS contribution from Sr is negligibly small in both cases indicating a high degree of ionic bonding between Sr and the host lattice. Close to the E_F (in the valence band) the density of state contribution from manganese and oxygen dominate for both modifications. The valence band consists of both oxygen *p* states and manganese *d* states, while the conduction band is dominated by manganese *d* states. We

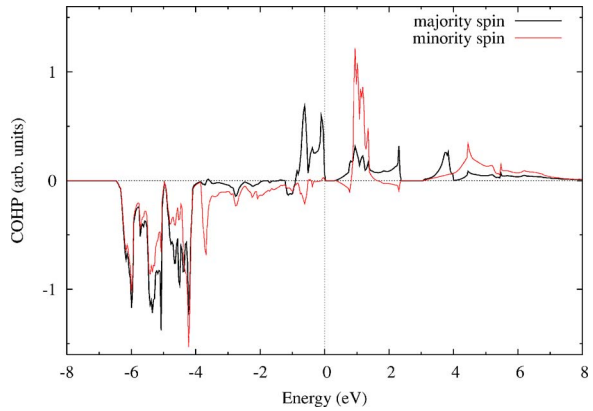

FIG. 10. (Color online) The crystal orbital Hamiltonian population for one Mn-O bond in *G*-type AF cubic $SrMnO_3$.

conclude that the band gap is of an intermediate character having both *p*-*d* charge transfer and *d*-*d* Mott-Hubbard characteristics. It can also be noted that even though the antiferromagnetic ground state has a d^3 configuration, there is a significant population of minority spin states in the valence band.

Several different features of the calculations point to significant covalent contributions to the bonding in $SrMnO_3$. One indication is the charges on the different ions obtained using the Bader charge population analysis.[56] For the hexagonal ground state the charges obtained for the Sr- and Mn-ions are 1.62 and 1.96, respectively. The O charges are 1.15 for the O ions in the face-sharing triangle and 1.27 for the other oxygen ions. The cubic ground state shows charges similar to those for the hexagonal ground state; 1.60, 1.97, and −1.21 for the Sr-, Mn-, and O-ions, respectively. We can again compare our results with results for closely related cubic $CaMnO_3$ calculated using the Hartree-Fock approach. These calculations give Mulliken charges 1.86, 2.17, and −1.34 for Ca, Mn, and O, respectively.[2] Such a low charge for Mn in formal oxidation state +4 has also been reported earlier for rutile-type MnO_2.[57]

Covalent contributions to the bonding are manifested also in detail of the electronic DoS. The manganese and oxygen DoS contributions show similarities in shape close to E_F indicating a degree of covalency of the bonds, both for cubic and for hexagonal $SrMnO_3$. Further details on the chemical bonding, supporting this view, are obtained from a crystal orbital Hamiltonian population analysis which shows bonding, antibonding, and nonbonding interactions between Mn and O. This is shown in Fig. 10 with the COHP for one Mn-O bond in cubic $SrMnO_3$. Strong Mn-O bonding interaction is evident in the region −6 to −4 eV of the valence band. Closer to the E_F there is close to zero overlap, which combined with a nonzero DoS indicate nonbonding states. Antibonding states are seen directly below and above E_F. Further details can be gained combining this information with the orbital-decomposed DoS.

The octahedral environment of the Mn atoms in cubic $SrMnO_3$ give rise to two and threefold degenerate, t_{2g} and e_g Mn *d* orbitals due to crystal field effects (see Fig. 11). In manganese oxides (i.e., MnO) the exchange splitting is larger

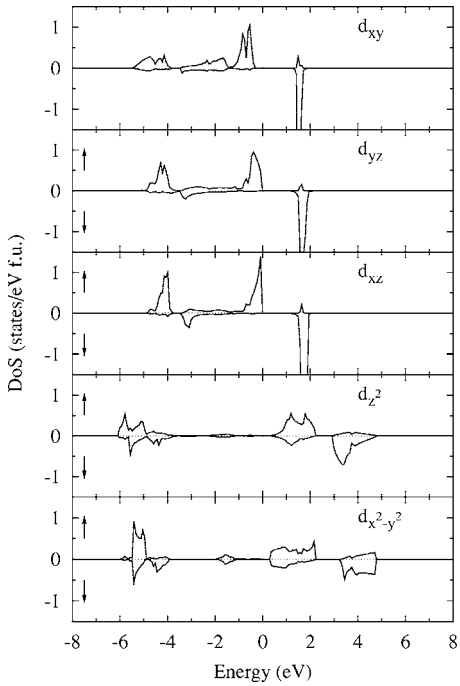

FIG. 11. The orbital-decomposed electronic density of state (the *d* orbitals only) of manganese in *G*-type AF cubic $SrMnO_3$.

than the ligand field splitting and both the valence band (VB) and the conduction band (CB) have a mixed e_g/t_{2g}-character.[58,59] From a purely ionic point of view the e_g orbitals pointing directly towards the neighboring O atoms are expected to contribute to the upper parts of both VB and CB bands, while the states of the t_{2g} orbitals that point between the O atoms would dominate at lower energy. In the present case however, the covalent character of the manganese-oxygen σ bond lowers the energy of a part of the e_g states. As a result some of the e_g states are presently lower in energy than the t_{2g} states in both the CB and VB in cubic $SrMnO_3$. These interactions give broader band features and more itinerant behavior for the e_g electrons. The less overlapping electrons in the t_{2g} orbitals, on the other hand, interact through weaker π bonds giving more localized states crucial for the magnetic properties. Even though these considerations explain the main features of the Mn-DoS it is clear that some down-spin levels are present even below E_F. In a purely ionic case, spin-down levels would not be occupied and the significant presence of minority spin *d* electrons in the VB indicates covalent interactions.

A last effect of the covalence is visible from the magnetic properties. As discussed, the observed moment is significantly lower than that expected from a spin only model (purely ionic). Furthermore, for the hypothetical ferromagnetic states there is considerable difference between the total moment of the cell and the magnetic moment on the manganese atoms alone. A significant magnetic moment is carried by the oxygen atoms due to back donation in the covalent bond. The same back donation is also expected for the AF states, but the magnetic moment of each oxygen atom is here cancelled out due to the AF ordering and thus this effect is less visible.

D. Stability of hexagonal versus cubic $SrMnO_3$

The main motivation for our study is to gain further understanding on the relative stability of cubic and hexagonal perovskite-type structures. While the ideal perovskite structure ABX_3 is cubic, the majority of the perovskites are distorted derivatives due to rotation or tilting of regular, rigid octahedra or due to the presence of distorted BX_6 octahedra. Octahedron tilting occurs when the size of the A-cation is too small for the 12-fold site within a BX_6 polyhedral framework. This tilting of the BX_6 polyhedra necessarily induces a distortion of the AX_{12} polyhedra which eventually will result in a decrease in the A-cation coordination number. The rotation/tilting does not disrupt the corner-sharing connectivity present in the ideal cubic perovskite. The structure of a perovskite-related oxide ABX_3 can, to some extent, be predicted from the tolerance factor

$$t = (r_A + r_X)/\sqrt{2}(r_B + r_X), \tag{4}$$

where r_A, r_B, and r_X are the ionic radii of the ions A, B, and X, respectively. $t=1$ corresponds to an ideal perovskite while a decreasing t corresponds to an increasing degree of distortion. A tolerance factor larger than unity, on the other hand, implies that the A cations are too large or the B cations too small for the compound to adopt the ideal cubic perovskite structure. For systems with large A cations, hexagonal perovskites form in which octahedra share faces resulting in chains along the hexagonal c axis. Thus, the formation of hexagonal perovskites is largely governed by the size misfits in the compound. While $BaMnO_3$ forms the 2H-hexagonal structure with face-sharing octahedra only, $CaMnO_3$ is close to cubic and contains only corner-sharing octahedra. $SrMnO_3$ containing intermediately sized Sr ions takes the four-layered hexagonal (4H) structure which may be seen as an intermediate containing both corner- and face-sharing octahedra. The hexagonal structures give more room to large A-site cations but, on the other hand, lead to short B-B distances along the face-sharing octahedra. While the distance between the manganese in two corner-sharing polyhedra in $SrMnO_3$ is 3.78 Å, the Mn-Mn distance over the common face is as short as 2.50 Å, hence comparable to the Mn-Mn distance (2.47 Å) in metallic γ-Mn (ideal cubic structure). The preference for hexagonal structures with increasing A-cation size is often explained by B-B metal bonding, see, e.g., Ref. 1. The analyses of the Mn contribution to the electronic density of state is, however, more difficult in the hexagonal case, since the different alignments of the octahedra makes a deconvolution of the total DoS into contributions from t_{2g} and e_g-like orbitals less straightforward. Instead, the charge density in the xz plane focusing on the Mn ions along the c axis is shown in Fig. 12. The expected Mn-Mn d-orbital overlap is minimal. Instead the charge density is dominated by covalent bonds between manganese and oxygen atoms. Face sharing of octahedra is unexpected in purely ionic oxides and this covalency of the Mn-O bonds is important for stabilizing the hexagonal $SrMnO_3$ structure at low temperatures. Covalency implies directional bonding that will reduce the Coulomb repulsion between the close metal atoms. The electrostatic Mn-Mn repulsion will also be reduced as the dimer formed

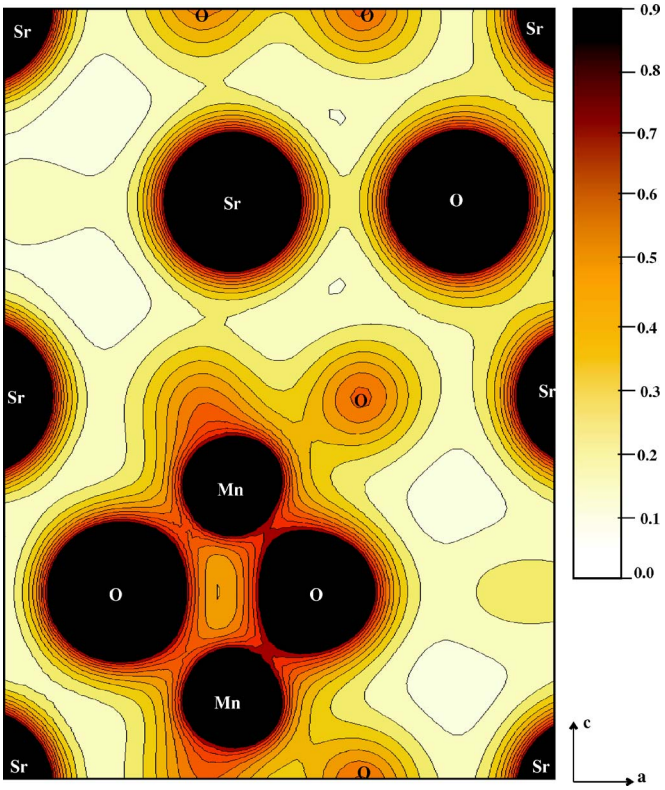

FIG. 12. (Color online) The charge density in the xz plane for hexagonal $SrMnO_3$, focusing on the interactions in the Mn_2O_9 dimer.

by face-sharing octahedra in 4H-$SrMnO_3$ allows displacement of the central B cation along the c axis.[60] For $SrMnO_3$ each Mn atom is displaced approximately 0.012 Å from the ideal position along the c axis (the experimental and calculated structure data are given in Table I). Furthermore, the lower charge of the oxygen atoms in the face-sharing triangle compared to those in the plane where the octahedra share corners (1.15 vs 1.27) reduces the O-O distance in the triangle; the O-O distance here being 2.516 Å while the O-O distance in the plane where the octahedra share corners is 2.744 Å. This negatively charged oxygen triangle effectively shields the repulsive interaction between the manganese atoms in the Mn_2O_9 dimer and facilitates the short Mn-Mn distance present in hexagonal $SrMnO_3$.

VI. SUMMARY

The electronic structure and magnetic properties of cubic and hexagonal $SrMnO_3$ are calculated using the generalized gradient approximation (GGA) within density functional theory. The structural and electronic properties are obtained for several different possible magnetic configurations. In both cases the ground states show AF ordering. For hexagonal $SrMnO_3$ AF coupling is found both within the Mn_2O_9 entities and between the Mn ions in the corner-sharing octahedra. A G-type AF ordering is most stable for the cubic polymorph. Band gaps at the Fermi energy are found for both polymorphs giving insulating properties at 0 K. The

nature of these band gaps are in the Zaanen, Sawatzky, Allen picture of intermediate character having both Mott-Hubbard and charge-transfer characteristics. While the bonding interactions involving Sr are found to be mainly ionic, there is a significant covalent contribution to the Mn-O bond. This covalency is very important for the stabilization of the hexagonal structure compared to the cubic polymorph. Two additional (partly related) factors are the displacement of the Mn atoms in the face-sharing octahedra along the *c* axis of the hexagonal structure and the charge transfer giving a lower charge on oxygen atoms in the oxygen triangle of the shared face compared to those in the plane where the octahedra share corners. The result is a contraction of the oxygen triangle that effectively shields the repulsive interaction between the manganese atoms in the Mn_2O_9 dimer. Bulk moduli for cubic and hexagonal $SrMnO_3$ are also calculated. Hexagonal $SrMnO_3$ is more compressible than cubic $SrMnO_3$ owing to the more open structure. The results obtained for hexagonal $SrMnO_3$ agree well with experimental results obtained by high-pressure powder x-ray diffraction.

ACKNOWLEDGMENTS

This work was funded by the Research Council of Norway (Project No. 155117/432). The Research Council of Norway (Programme for Supercomputing) has also supported the work through a grant of computing time.

*Corresponding author. Electronic address: svein.stolen@kjemi.uio.no

[1] R. H. Mitchell, *Perovskites: Modern and Ancient* (Almaz Press, Ontario, Canada, 2002).
[2] F. F. Fava, P. D'Arco, R. Orlando, and R. Dovesi, J. Phys.: Condens. Matter **9**, 489 (1997).
[3] B. L. Chamberland, A. W. Sleight, and J. F. Weiher, J. Solid State Chem. **1**, 506 (1970).
[4] Y. Syono, S. I. Akimoto, and K. Kohn, J. Phys. Soc. Jpn. **26**, 993 (1969).
[5] T. Negas, J. Solid State Chem. **7**, 85 (1973).
[6] L. Rørmark, A. B. Mørch, K. Wiik, S. Stølen, and T. Grande, Chem. Mater. **13**, 4005 (2001).
[7] P. D. Battle, T. C. Gibb, and C. W. Jones, J. Solid State Chem. **74**, 60 (1988).
[8] E. O. Wollan and W. C. Koehler, Phys. Rev. **100**, 545 (1955).
[9] T. Takeda and S. Ohara, J. Phys. Soc. Jpn. **37**, 275 (1974).
[10] K. Kikuchi, H. Chiba, M. Kikuchi, and Y. Syono, J. Solid State Chem. **146**, 1 (1999).
[11] O. Chmaissem, B. Dabrowski, S. Kolesnik, J. Mais, D. E. Brown, R. Kruk, P. Prior, B. Pyles, and J. D. Jorgensen, Phys. Rev. B **64**, 134412 (2001).
[12] T. Negas and R. S. Roth, J. Solid State Chem. **1**, 409 (1970).
[13] S. Hashimoto and H. Iwahara, J. Electroceram. **4**, 225 (2000).
[14] K. J. Lee and E. Iguchi, J. Solid State Chem. **114**, 242 (1995).
[15] J. Zaanen, G. A. Sawatzky, and J. W. Allen, Phys. Rev. Lett. **55**, 418 (1985).
[16] W. C. Mackrodt and E. A. Williamson, Ber. Bunsenges. Phys. Chem. **101**, 1215 (1997).
[17] M. Abbate, F. M. F. de Groot, J. C. Fuggle, A. Fujimori, O. Strebel, F. Lopez, M. Domke, G. Kaindl, G. A. Sawatzky, M. Takano, Y. Takeda, H. Eisaki, and S. Uchida, Phys. Rev. B **46**, 4511 (1992).
[18] A. Chainani, M. Mathew, and D. D. Sarma, Phys. Rev. B **47**, 15397 (1993).
[19] T. Saitoh, A. E. Bocquet, T. Mizokawa, H. Namatame, A. Fujimori, M. Abbate, Y. Takeda, and M. Takano, Phys. Rev. B **51**, 13942 (1995).
[20] G. Zampieri, F. Prado, A. Caneiro, J. Briatico, M. T. Causa, M. Tovar, B. Alascio, M. Abbate, and E. Morikawa, Phys. Rev. B **58**, 3755 (1998).
[21] Z. Fang, I. V. Solovyev, and K. Terakura, Phys. Rev. Lett. **84**, 3169 (2000).
[22] S. Satpathy, Z. S. Popovic, and F. R. Vukajlovic, Phys. Rev. Lett. **76**, 960 (1996).
[23] D. Fuks, S. Dorfman, J. Felsteiner, L. Bakaleinikov, A. Gordon, and E. A. Kotomin, Solid State Ionics **173**, 107 (2004).
[24] K. Kuroda, N. Ishizawa, N. Mizutani, and M. Kato, J. Solid State Chem. **38**, 297 (1981).
[25] J. J. Adkin and M. A. Hayward, J. Solid State Chem. **179**, 70 (2006).
[26] A. J. Jacobson and A. J. W. Horrox, Acta Crystallogr., Sect. B: Struct. Crystallogr. Cryst. Chem. **32**, 1003 (1976).
[27] E. J. Cussen, J. Sloan, J. F. Vente, P. D. Battle, and T. C. Gibb, Inorg. Chem. **37**, 6071 (1998).
[28] N. A. Jordan and P. D. Battle, J. Mater. Chem. **13**, 2220 (2003).
[29] H. Fjellvåg, E. Gulbrandsen, S. Aasland, A. Olsen, and B. C. Hauback, J. Solid State Chem. **124**, 190 (1996).
[30] P. E. Blöchl, Phys. Rev. B **50**, 17953 (1994).
[31] P. Hohenberg and W. Kohn, Phys. Rev. **136**, B864 (1964).
[32] W. Kohn and L. J. Sham, Phys. Rev. **140**, A1133 (1965).
[33] G. Kresse and J. Furthmüller, Phys. Rev. B **54**, 11169 (1996).
[34] J. P. Perdew, K. Burke, and M. Ernzerhof, Phys. Rev. Lett. **77**, 3865 (1996).
[35] F. D. Murnaghan, Proc. Natl. Acad. Sci. U.S.A. **30**, 244 (1944).
[36] O. L. Anderson, *Equations of State of Solids for Geophysics and Ceramic Science* (Oxford University Press, New York, USA, 1995).
[37] R. Dronskowski and P. E. Blöchl, J. Phys. Chem. **97**, 8617 (1993).
[38] O. K. Andersen, Phys. Rev. B **12**, 3060 (1975).
[39] O. K. Andersen and O. Jepsen, Phys. Rev. Lett. **53**, 2571 (1984).
[40] R. L. Mills, B. Olinger, and D. T. Cromer, J. Chem. Phys. **84**, 2837 (1986).
[41] W. E. Streib, T. H. Jordan, and W. N. Lipscomb, J. Chem. Phys. **37**, 2962 (1962).
[42] D. T. Cromer, R. L. Mills, D. Schiferl, and L. A. Schwalbe, Acta Crystallogr., Sect. B: Struct. Crystallogr. Cryst. Chem. **37**, 8 (1981).
[43] H. Olijnyk, J. Chem. Phys. **93**, 8968 (1990).
[44] H. K. Mao, J. Xu, and P. M. Bell, J. Geophys. Res. **91**, 4673 (1986).

[45] A. P. Hammersley, S. O. Svensson, M. Hanfland, A. N. Fitch, and D. Hausermann, High Press. Res. **14**, 235 (1996).
[46] W. E. Pickett and D. J. Singh, Phys. Rev. B **53**, 1146 (1996).
[47] M. Nicastro and C. H. Patterson, Phys. Rev. B **65**, 205111 (2002).
[48] S. F. Matar, Prog. Solid State Chem. **31**, 239 (2003).
[49] S. F. Matar, F. Studer, B. Siberchicot, M. A. Subramanian, G. Demazeau, and J. Etourneau, Eur. Phys. J.: Appl. Phys. **4**, 143 (1998).
[50] J. B. Goodenough, *Magnetism and the Chemical Bond* (Interscience-Wiley, New York, 1963).
[51] J. Kanamori, J. Phys. Chem. Solids **10**, 87 (1959).
[52] P. W. Anderson, in *Solid State Physics*, edited by F. Seitz and D. Turnbull (Academic Press, New York, 1963), Vol. 14, p. 99.
[53] W. Geertsma and D. Khomskii, Phys. Rev. B **54**, 3011 (1996).
[54] A. M. Daré, R. Hayn, and J. L. Richard, Europhys. Lett. **61**, 803 (2003).
[55] R. Vidya, P. Ravindran, H. Fjellvåg, A. Kjekshus, and O. Eriksson, Phys. Rev. Lett. **91**, 186404 (2003).
[56] G. Henkelman, A. Arnaldsson, and H. Jónsson, Comput. Mater. Sci. **36**, 354 (2006).
[57] W. C. Mackrodt and E. A. Williamson, J. Chem. Soc., Faraday Trans. **93**, 3295 (1997).
[58] K. Terakura, T. Oguchi, A. R. Williams, and J. Kübler, Phys. Rev. B **30**, 4734 (1984).
[59] M. D. Towler, N. L. Allan, N. M. Harrison, V. R. Saunders, W. C. Mackrodt, and E. Aprà, Phys. Rev. B **50**, 5041 (1994).
[60] J. B. Goodenough and J. S. Zhou, Chem. Mater. **10**, 2980 (1998).